Applied Surface Science 257 (2011) 9251–9259

Contents lists available at ScienceDirect

Applied Surface Science

journal homepage: www.elsevier.com/locate/apsusc

Microstructure and surface mechanical properties of pulse electrodeposited nickel

A. Ul-Hamid*, H. Dafalla, A. Quddus, H. Saricimen, L.M. Al-Hadhrami

Center of Research Excellence in Corrosion (CoRE-C), Research Institute, King Fahd University of Petroleum & Minerals, P.O. Box 1073, Dhahran 31261, Saudi Arabia

ARTICLE INFO

Article history:
Received 2 September 2010
Received in revised form
15 December 2010
Accepted 25 April 2011
Available online 16 June 2011

Keywords:
Pulse electrodeposition
Nickel
Microstructure
Nanoindentation

ABSTRACT

The surface of carbon steel was modified by electrochemical deposition of Ni in a standard Watt's bath using dc and pulse plating electrodeposition. The aim was to compare the microstructure and surface mechanical properties of the deposit obtained by both techniques. Materials characterization was conducted using field emission scanning electron microscope fitted with scanning transmission electron detector, atomic force microscope and X-ray diffractometer. Nanoindentation hardness, elastic modulus, adhesion, coefficients of friction and wear rates were determined for both dc and pulse electrodeposits. Experimental results indicate that pulse electrodeposition produced finer Ni grains compared to dc plating. Size of Ni grains increased with deposition. Both dc and pulse deposition resulted in grain growth in preferred (2 0 0) orientation. However, presence of Ni (1 1 1) grains increased in deposits produced by pulse deposition. Pulse plated Ni exhibited higher hardness, creep and coefficient of friction and lower modulus of elasticity compared to dc plated Ni.

1. Introduction

Nickel is extensively used in the development of coatings with an aim to improve the surface properties of a large number of alloys. Nickel coating protects metal surface from environmental degradation and makes for a hard and wear-resistant surface. Nickel coatings also carry aesthetic value and satisfy decorative needs. Nickel deposition can be carried out using electrolytic or electroless technique, each of which provides certain benefits. Electroless plating can be relatively expensive and time-intensive [1,2].

Parameters employed during electrolytic technique control the grain size, morphology and texture of electrodeposited Ni, which in turn affect the surface properties of the deposit. Both dc [3–6] and pulse [7–14] electrodeposition has been used to deposit Ni in order to improve the corrosion, tribological and aesthetic properties of products used in various applications. Pulse electrodeposition has become increasingly popular due to its cost effectiveness combined with its ability to provide high current density, power and controlled pulse waveforms [15]. Pulse electrodeposition can reduce porosity and improve corrosion resistance of Ni deposits compared to dc plating [16]. Wear resistance of electrodeposited Ni has also been reported to increase with decreasing grain size [10].

During pulse plating, current is applied as a repetitive square wave (on-off plating) while peak current density, pulse on-time and pulse off-time are closely controlled. Nucleation occurs at increased rate while grain growth is suppressed resulting in fine grained coatings compared to those obtained by dc electrodeposition. Nanostructured coatings with less than 100 nm grain size can greatly improve material properties compared to their conventional counterparts. Progress in the development of nanostructured coatings can lead to potential improvements in corrosion, wear, strength, erosion and other properties useful for various applications. Therefore, it is necessary to study the properties of coatings produced by pulse electrodeposition to provide a comparison for materials produced by conventional dc deposition technique.

In the present study, Ni was deposited on carbon steel using dc and pulse electrodeposition. The surface morphology of Ni electrodeposits was examined using scanning electron microscopy (SEM) and atomic force microscopy (AFM). Microstructure of the Ni deposits was characterized using scanning transmission electron microscope (STEM) detector mounted on scanning electron microscope combined with focused ion beam instrument. Surface mechanical properties were evaluated by measuring the nanohardness, microscratch, and coefficients of friction characteristics of Ni. It was the aim of this study to compare the surface mechanical properties of Ni electrodeposits obtained by dc and pulse electrodeposition and also to examine the effect of microstructure on the surface properties of electrodeposited Ni.

* Corresponding author. Tel.: +966 3 8602017; fax: +966 3 8603996.
E-mail address: anwar@kfupm.edu.sa (A. Ul-Hamid).

0169-4332/$ – see front matter © 2011 Elsevier B.V. All rights reserved.
doi:10.1016/j.apsusc.2011.04.120

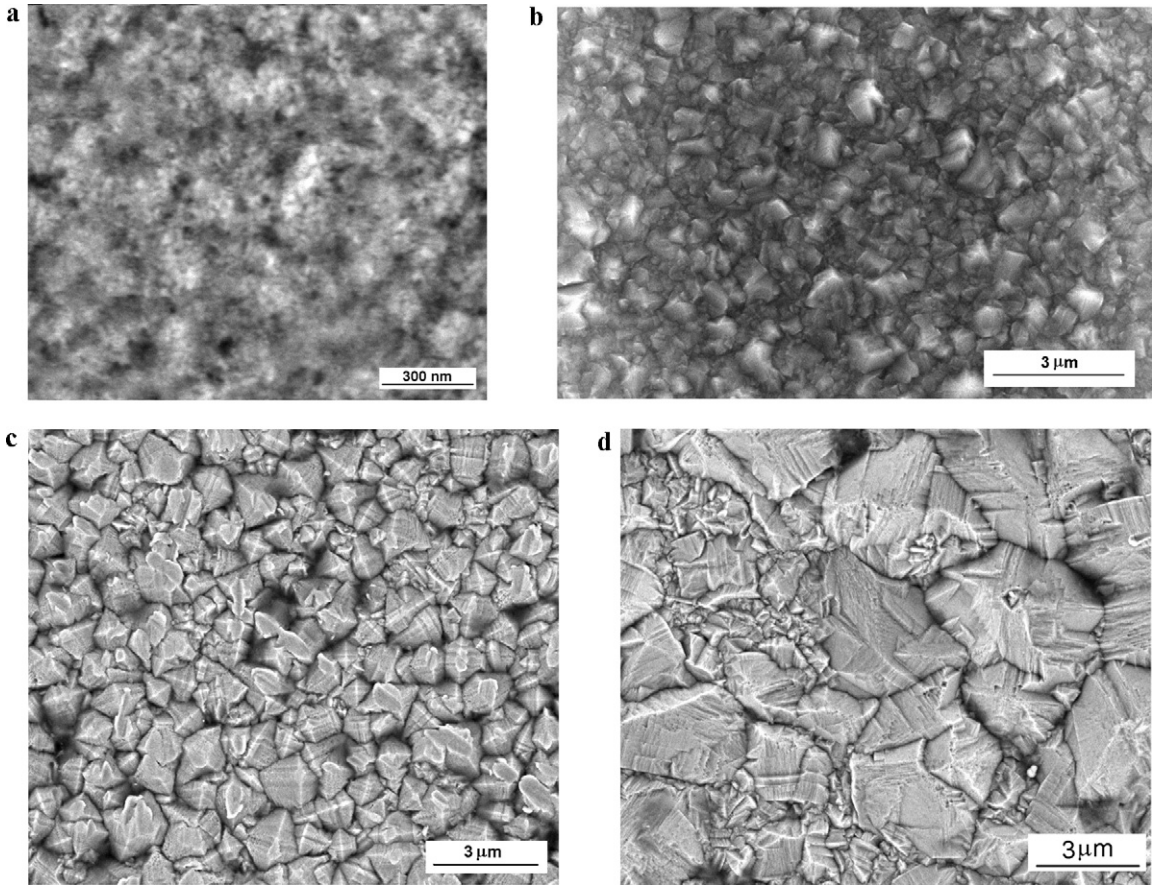

Fig. 1. Surface morphologies of Ni after (a) 1 min, (b) 10 min, (c) 20 min and (d) 60 min of dc electrodeposition.

2. Experimental

2.1. Electrodeposition

Plain carbon steel samples (20 mm × 10 mm × 3 mm) were metallographically ground and polished to a surface finish of 1 μm. They were degreased with acetone and rinsed with distilled water. The composition of Watt's bath used in this study was $NiSO_4{\cdot}6H_2O$ (250 g), $NiCl_2{\cdot}6H_2O$ (50 g) and H_3BO_3 (35 g) per liter of water. Pure Ni was used as anode and carbon steel as cathode during electrodeposition. The pH and temperature of the electrolyte were maintained at 3.6 and 45 °C, respectively. Current density used for dc plating was 50 mA/cm^2. Pulse electrodeposition was performed at different peak current densities of 520, 690, 860 and 1030 mA/cm^2 for durations of 15–60 min. Pulse on-time (T_{on}) and off-time (T_{off}) were kept at 2 and 10 ms, respectively.

2.2. Materials characterization and grain size, texture and residual stress measurements

Field emission scanning electron microscope (SEM) combined with focused ion beam instrument equipped with scanning trans-

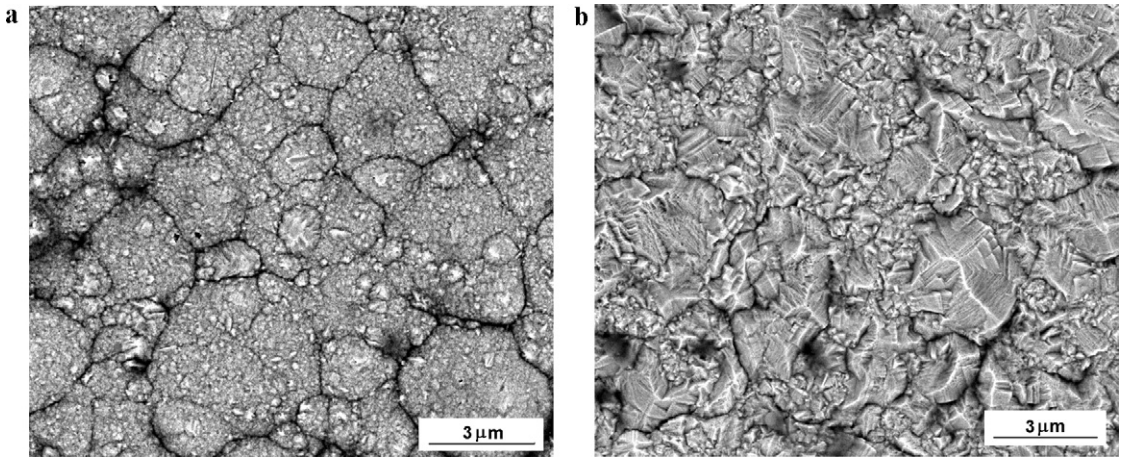

Fig. 2. Surface morphologies of Ni deposited at peak current density of 690 mA/cm^2 after (a) 15 min and (b) 60 min of pulse electrodeposition.

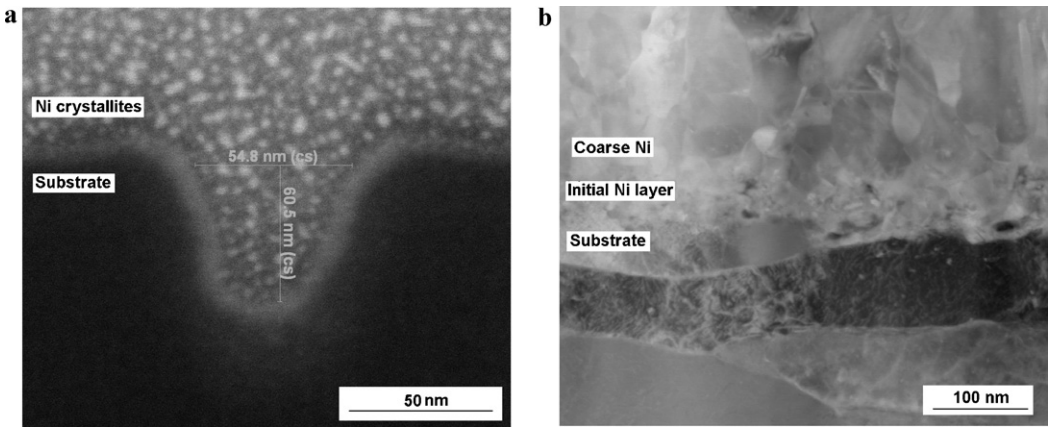

Fig. 3. (a and b) Cross-sectional HAADF images showing fine Ni crystallites formed at the initial stage of electrodeposition.

mission electron microscope (STEM) detector and atomic force microscope (AFM-contact mode) was used to examine the surface morphology and microstructure of electrodeposited Ni. An X-ray diffractometer equipped with a monochromator was used to examine the grain size, texture and residual stress of Ni deposits. The diffraction spectra were generated using Cu Kα radiation (λ = 1.54184 Å) source operating at 40 kV and 40 mA. Phase identification and crystallite size measurements were carried out using a Bragg–Brentano (BB) configuration with θ/θ scan axis. Crystallite size was determined using both Williamson–Hall and whole-powder-pattern-decomposition (WPPF) pattern decomposition by Rietveld method. Williamson–Hall method combines Scherrer equation for size broadening and Stokes and Wilson expression for strain broadening as follows:

$$B \cdot \cos(\theta) = \frac{k\lambda}{D} + \eta \cdot \sin\theta,$$

A straight line is obtained when $B \cdot \cos(\theta)$ is plotted against $\sin(\theta)$ with slope η and intercept $k\lambda/D$. The value of η is the strain in the crystallites while the value of D is the size of the crystallites. The constant k is typically close to unity and ranges from 0.8 to 1.39.

Pole figure and texture analysis was undertaken with BB configuration at alpha/beta axis. Residual stress measurements were conducted at parallel beam configuration with $2\theta/\theta$ axis on Ni (3 1 1) planes using iso-inclination scanning (ψ angle).

2.3. Surface mechanical properties

Details of experimental setup used for nanoindentation, microscratch and pin-on-disc tribometer tests have been reported elsewhere [17]. Creep (C_S) of the sample was calculated as follows:

$$C_S = \frac{h_2 - h_1}{h_1}$$

where h_1 is the indentation depth at the time of reaching the test force, h_2 is the indentation depth at the time of holding the test force.

During tribometer test, the linear speed of the disc was maintained at 5 cm/s and total number of laps was fixed at 5000. The radius was 3.5 mm and total sliding distance was approximately 110 m.

3. Results and discussion

3.1. Evolution of microstructure

3.1.1. Direct current electrodeposition

Relatively uniform, continuous and adherent Ni deposit was obtained at a current density of 50 mA/cm^2 after 10 min of deposition. Higher than optimal temperature resulted in non-adherent and flaky deposits while lower temperature led to irregular and inconsistent deposits that failed to cover the entire surface of the sample. Increased pH levels of the bath gave rise to cracked, flaky and blackened deposits. Surface morphologies of Ni electrodeposited for 10, 15 and 60 min are shown in Fig. 1. Initial Ni crystallites deposited at the steel cathode surface are small in size as shown in Fig. 1a. After 10 min of deposition, Ni grains grow to sub-micron size (see Fig. 1b). After 20 min, maximum size of Ni grains can be as much as 2 μm as shown in Fig. 1c. Deposition of

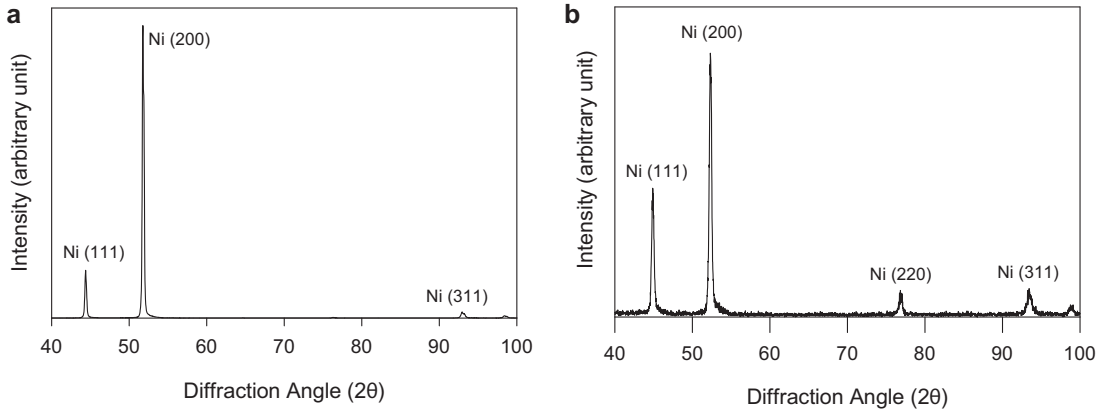

Fig. 4. X-ray diffraction spectra obtained from (a) dc and (b) pulse electroplated Ni.

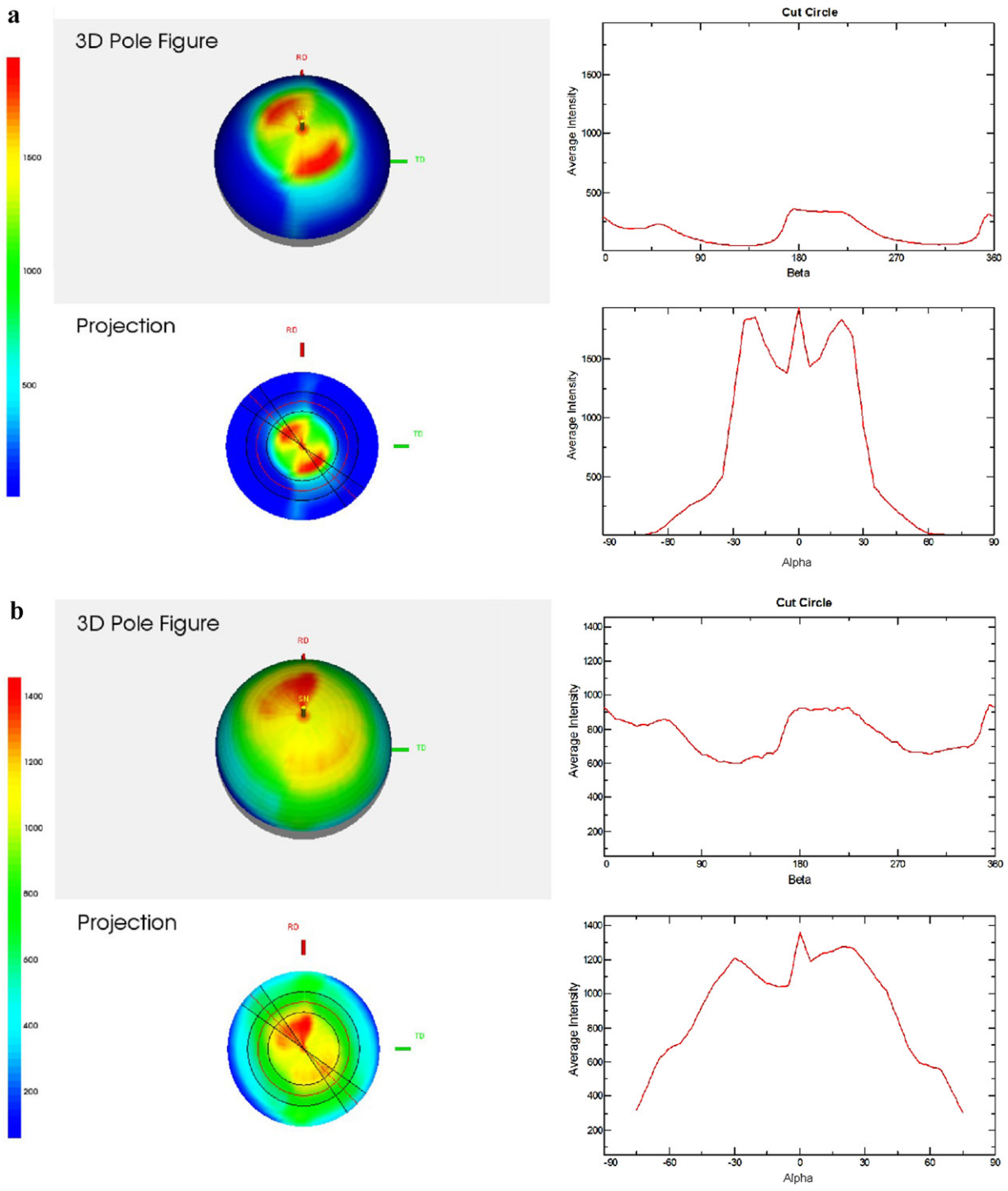

Fig. 5. Pole figures for pulse plated Ni in (a) 1 1 1 and (b) 2 0 0 directions.

1 h can produce Ni grains of up to 3 μm, as seen in Fig. 1d. It can be seen from the SEM micrographs that an increase in deposition time changes the crystal orientation from random (Fig. 1b) to preferred [2 0 0] texture (Fig. 1d).

The concentration of Ni^{2+} ions at the cathode surface is gradually diminished due to continuous deposition resulting in a progressively coarser grain deposition with time [18]. The rate of grain coarsening, however, decreases with time. Eventually Ni^{2+} concentration at the cathode surface stabilizes inducing stability in the deposit grain size. Fig. 1d clearly shows that dc electrodeposition at this current density results in compact structures where coarse pyramidal grains are accompanied by fine grains with the same morphology and the crevices around the grains are not present.

3.1.2. Pulse electrodeposition

Fig. 2 shows surface morphologies of Ni produced by pulse electrodeposition. Colonies constituting fine equiaxed grains of Ni are visible separated by crevices after 15 min of deposition as shown in Fig. 2a. After 1 h of deposition, most of the fine equiaxed are replaced by coarse pyramidal grains and appearance of crevices diminish significantly due to the formation of fine faceted grains

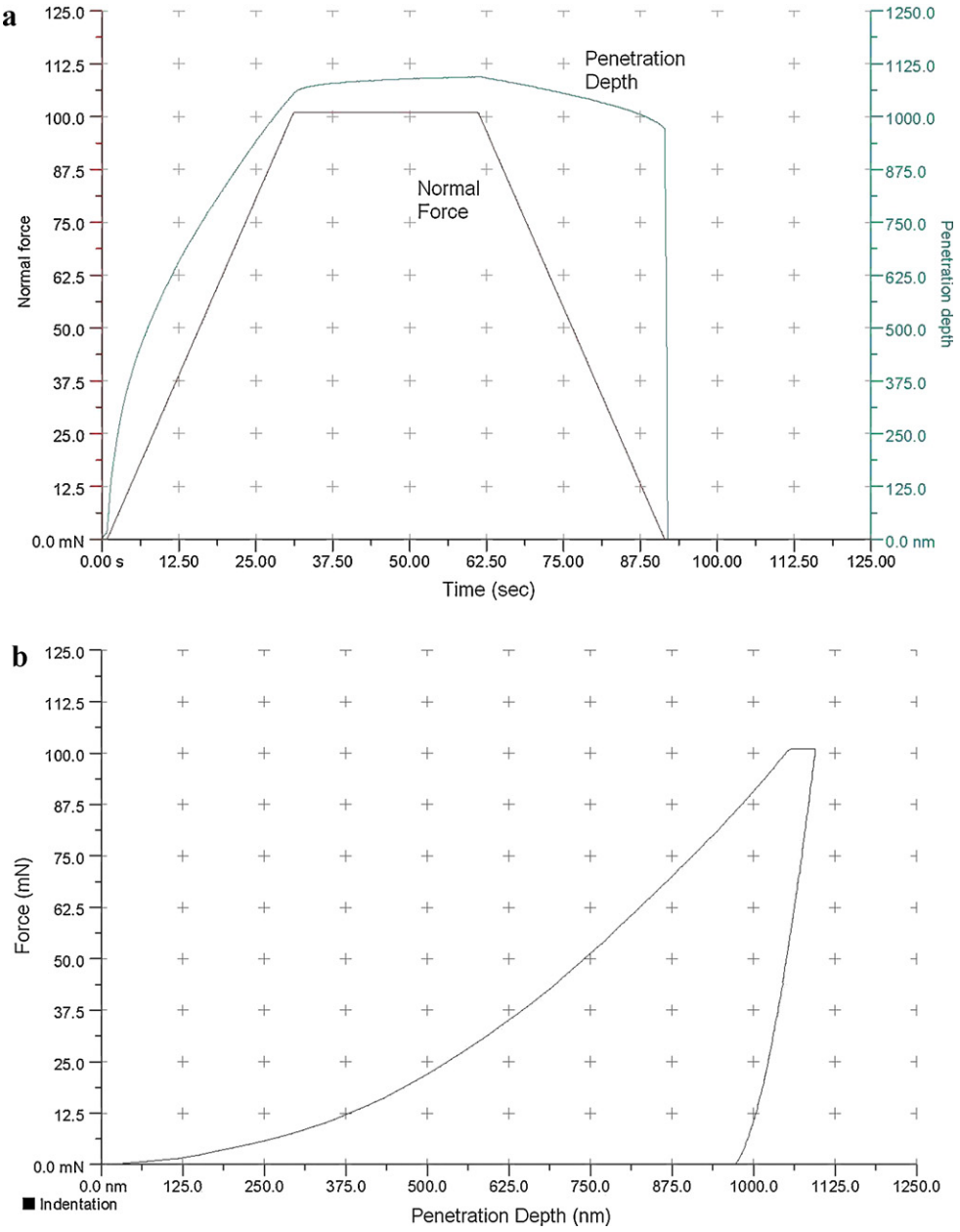

Fig. 6. Load displacement curves obtained from pulse electrodeposited Ni showing (a) normal force and penetration depth vs. time of indentation and (b) normal force vs. depth of penetration.

(see Fig. 2c). Thickness of Ni deposit after 1 h of deposition was 120 μm.

Cross-sectional high angle annular dark field (HAADF) images illustrating typical microstructure of Ni electrodeposit formed at the deposit–substrate interface are shown in Fig. 3a and b. It can be seen that the Ni crystallites deposited at the alloy surface at the very beginning of electrodeposition are ≤10 nm in size as shown in Fig. 3a. This is about 4 times smaller compared with the initial crystallite size deposited during dc plating. It can be seen in Fig. 3a that the fine layer of Ni crystallites deposited at the steel surface is only ≈50 nm in thickness. It is followed by another layer where average size of Ni grains was observed to be ≈50 nm. It is clear from these images that Ni grain size becomes coarser with deposition time. Microstructure of Ni deposit is characterized by high angle grain boundaries. Coarser Ni grains exhibited columnar morphology. Presence of twins within Ni grains was also observed indicating low stacking fault energy of Ni during electrodeposition [19]. Substrate immediately beneath the Ni deposit shows presence of dislocations that can indicate stresses generated due to hydrogen evolution during Ni deposition [20]. Size of Ni grains initially deposited at the substrate surface influence subsequent grain morphology and texture which in turn affects the stability of Ni deposit [21]. A comparison of Fig. 2c and Fig. 1d shows that the average number of coarse grains after 1 h of pulse electrodeposition is lower compared to that obtained for dc electrodeposition for the same duration of deposition. Finer grain size distribution of Ni obtained using pulse deposition can be partially attributed to the fine-grained layer (10 nm grain size) initially obtained at the substrate surface. It was also observed in the present study that fine grained Ni obtained using pulse electrodeposition resulted in deposits that were relatively more stable and adherent compared to those obtained using dc electrodeposition. This could be partially attributed to low level of porosity associated with fine grained Ni deposits [22].

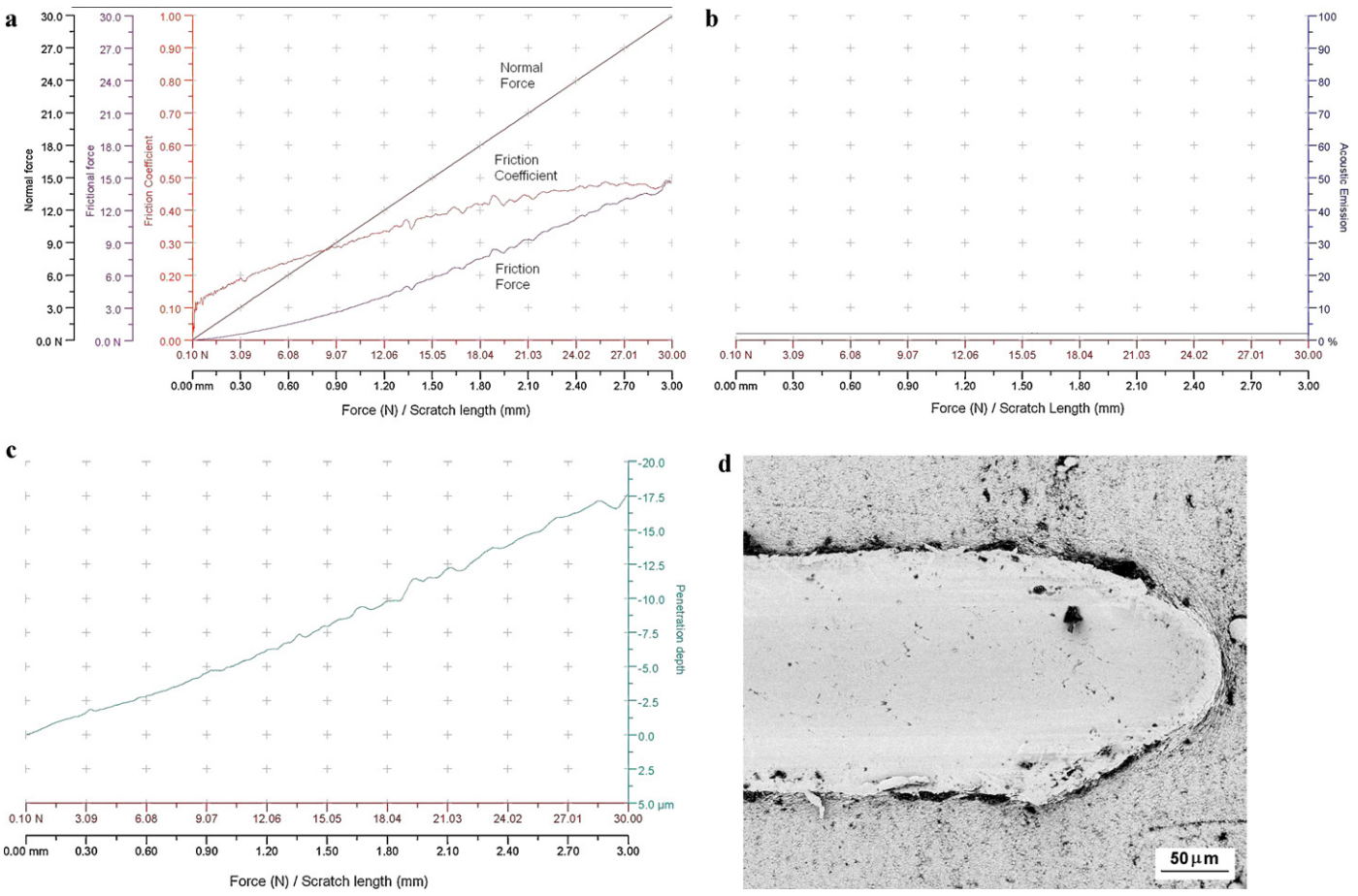

Fig. 7. Microscratch test of pulse electrodeposited Ni showing graphs of (a) normal force, friction force and coefficient of friction, (b) acoustic emission and (c) penetration depth plotted against length of scratch. (d) SEM micrograph of the scratch.

3.2. Grain size, texture and residual stress measurements

X-ray diffraction patterns obtained from dc and pulse electroplated samples are shown in Fig. 4a and b, respectively. The dc plated sample shows strong preferred [2 0 0] orientation (see Fig. 4a) corresponding to coarse faceted pyramidal morphology. Maximum grain size for this sample was measured at 3 μm after 1 h of deposition. Pulse electrodeposited Ni maintains preferred growth orientation of (2 0 0) planes (see Fig. 4b). Preferred texture along [2 0 0] direction in electrodeposited Ni has been reported in the literature [23]. However, the spectrum for pulse deposited Ni shows higher intensity ratio of (1 1 1) to (2 0 0) peaks compared with dc plated sample. Since isotropic polycrystalline Ni exhibits strong [1 1 1] random orientation, increased intensity of Ni (1 1 1) planes in the XRD spectrum obtained from pulsed deposited sample is thought to correspond to higher degree of fine equiaxed grains present within this sample. It is believed that pulse deposition results in an increase in the growth of Ni grains along [1 1 1] direction.

Pole figures of pulse electrodeposited Ni in [1 1 1] and [2 0 0] directions depicting crystal orientation are shown in Fig. 5a and b. It indicates that pulse Ni deposit constitutes grain growth in both orientations. Average grain size of Ni for this sample pulse deposited at a peak current density of 690 mA/cm^2 for 15 min was 25 nm measured using X-ray diffraction technique. The values of residual stress are summarized in Table 1. The residual stress in pulse electrodeposited Ni was measured as −207 MPa (compressive) using iso-inclination XRD method. Residual stress in electrodeposited polycrystalline Ni measured by XRD has been reported as 143 and −130 MPa [20,24]. Reported values for pulse deposits with 10 nm grain size vary between −452 and −842 MPa [20] depending on deposit–substrate lattice misfit as well as plating conditions such as bath composition and current density. Stresses in pulse deposits are generally higher than in dc deposits owing to the ability of pulse deposition to reduce hydrogenation of deposits [20].

3.3. Surface mechanical properties

Typical load–displacement curves obtained from nanoindentation test of Ni deposit are shown in Fig. 6. The applied normal force (load) and the penetration depth of the indenter (displacement) are plotted against time in Fig. 6a. The normal force vs. penetration depth for the same indent is plotted in Fig. 6b. These curves are used to calculate mechanical properties of the material using Oliver & Pharr (O & P) method [25] as shown in Table 1. The results show that the nanohardness obtained from pulse electrodeposited Ni is higher than dc electrodeposited Ni. This is thought to be due to the fine grain structure of Ni obtained due to pulse deposition. Grain size difference also resulted in pulse electrodeposited Ni having slightly higher degree of creep compared to dc plated Ni as calculated from nanoindentation tests (see Table 1). In addition, modulus of elasticity calculated for pulse Ni was lower than dc plated Ni.

Microscratch test results for pulse electrodeposited Ni at 30 N load are shown in Fig. 7a–d. Normal force, friction force and coefficient of friction are plotted against the displacement in a graph shown in Fig. 7a. Acoustic emission and penetration depth are plotted in Fig. 7b and c, respectively. The acoustic emission does not record any signal indicating that cracking of coating does not occur

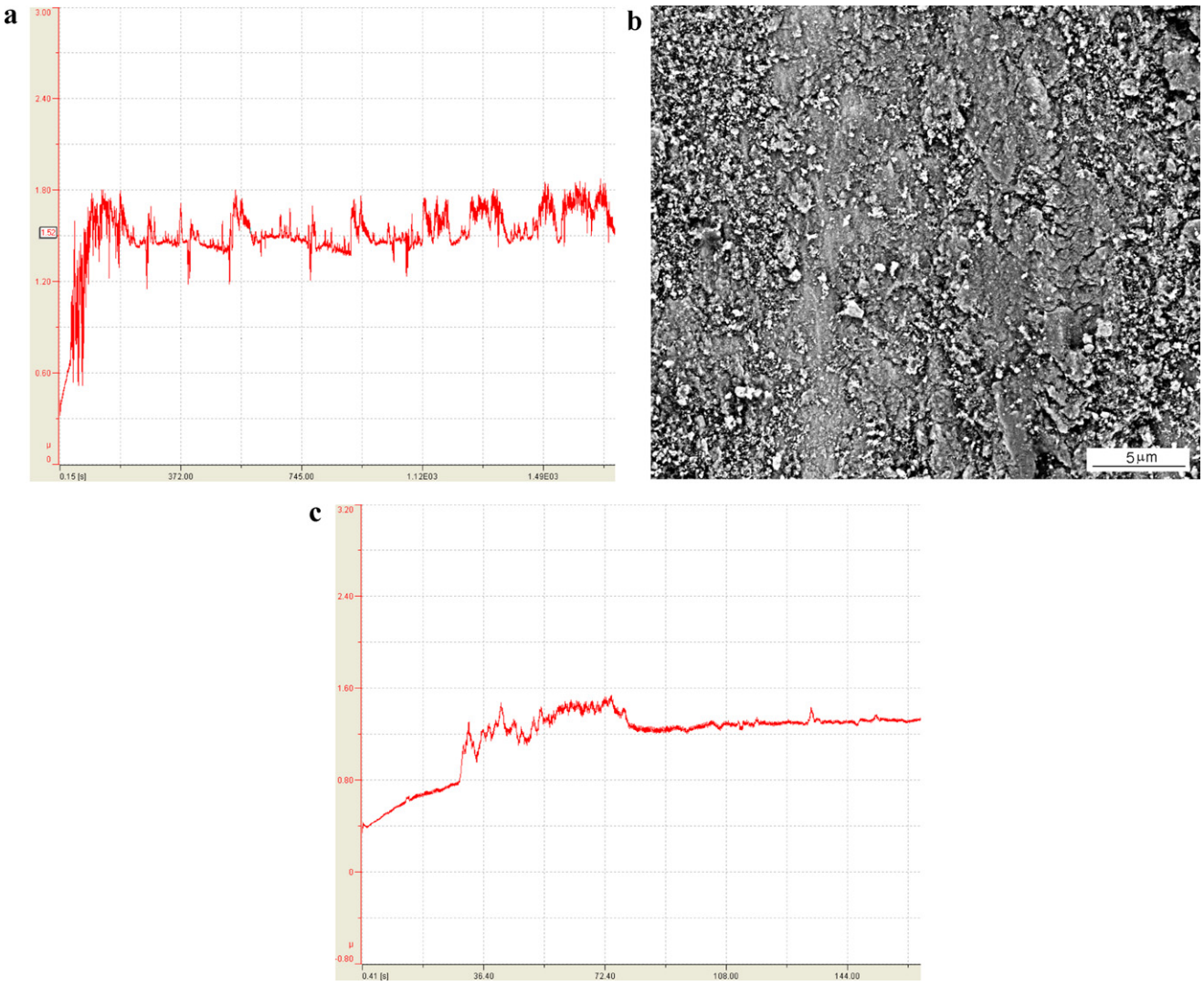

Fig. 8. (a) Plot of friction of coefficient with time for 5000 laps and (b) surface morphology for pulse plated Ni. (c) Friction of coefficient plot for dc plated Ni.

at a load of 30 N. This is confirmed by the SEM macrograph (see Fig. 7d) showing the end of the scratch region where electrodeposited Ni is smeared by sliding action of the indenter giving rise to side ridges. No signs of cracking, chipping or de-cohesion of the Ni are visible which is indicative of an adherent deposit.

Plots obtained for pulse and dc electrodeposited Ni using pin-on-disc test on tribometer are shown in Fig. 8a and b, respectively. Relatively high values of coefficient of friction (μ) were obtained for both pulse and dc electrodeposited Ni as shown in Table 1. Nickel deposited by pulse method shows slightly higher friction

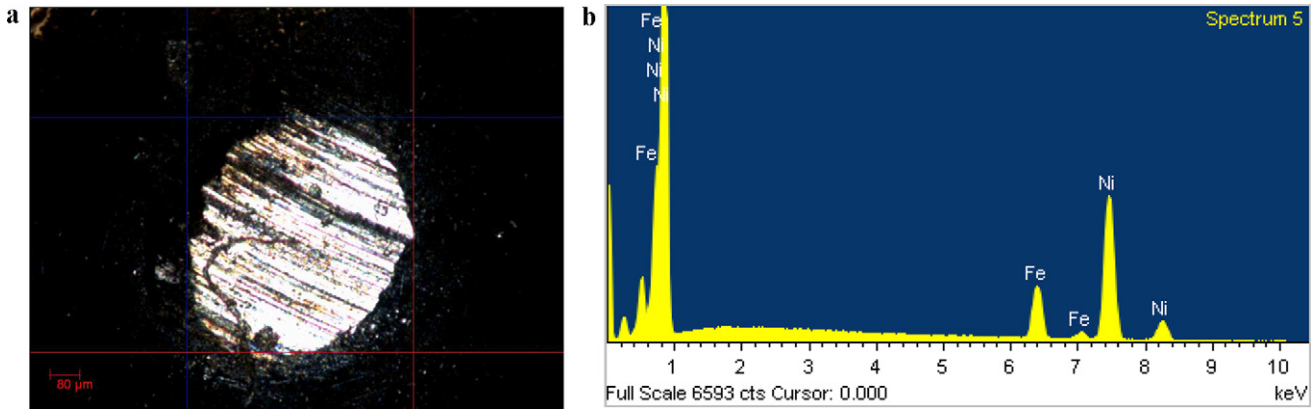

Fig. 9. (a) Optical image showing worn area of ball used in tribometer test. (b) SEM-EDS spectrum obtained from wear track formed on Ni deposit showing the presence of Fe removed from steel ball.

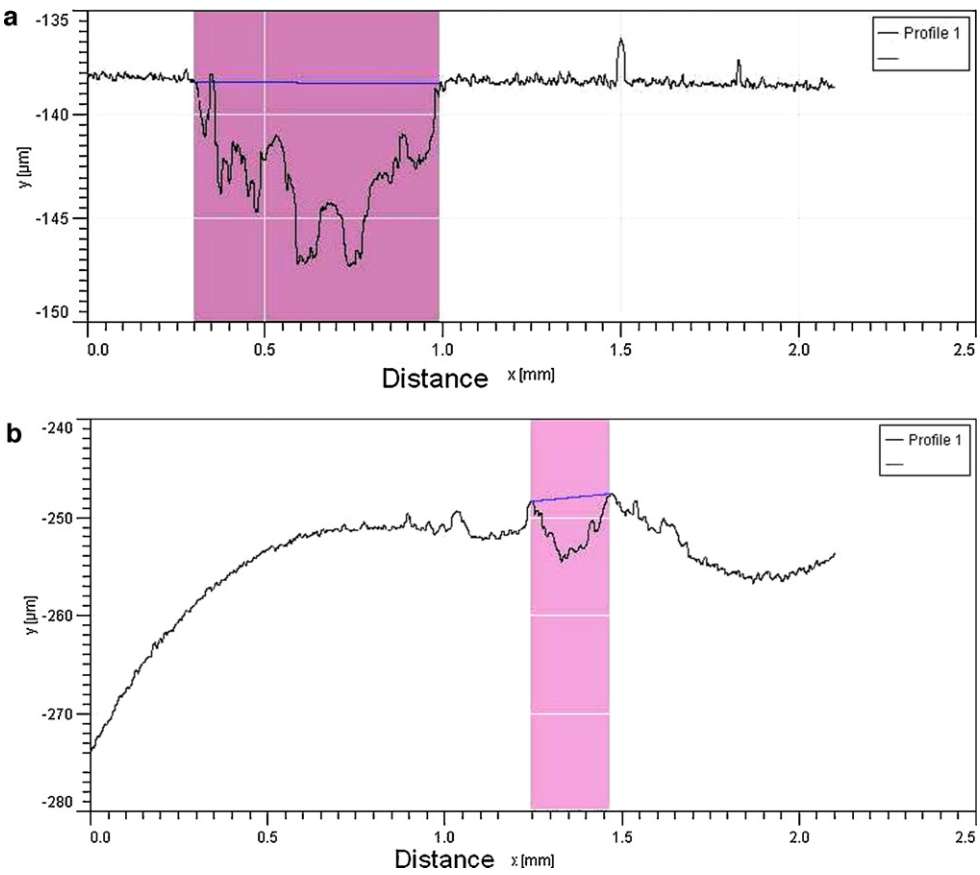

Fig. 10. Cross-sectional profiles of wear tracks for (a) pulse and (b) dc plated Ni samples showing area of worn tracks.

coefficients compared to dc method. It can be seen in Fig. 8a that significant fluctuations occur during the test for pulse deposited Ni. This is caused by the deposition of the ball material on the sample. Significant wear on the ball was also observed. Plot in Fig. 8a shows a 'running-in time' for friction measurement at the beginning. Friction coefficient value starts at a low value of 0.36 and increases steadily up to 0.68. At 35 s, the deposits of materials on the surface create a regime of fluctuations of friction coefficient values. The smooth surface is transformed into an additional third body layer, probably comprising deposits of the worn ball and wear of the coating. After 180 s, the friction coefficient starts to be more constant in average value. Subsequently, an average value of 1.52 is reached which is considered to be a high value of friction coefficient. Fig. 8b shows the morphology of the wear track formed on pulse electrodeposited Ni indicating surface roughness resulting from material removal during tribometer test.

For dc pulsed samples, 'running-in time' for friction measurement was also observed at the beginning as seen in Fig. 8c. Friction coefficient value starts at a low value of 0.35 and increases steadily up to 0.78 at 30 s. At 30 s, there is a sharp increase. But around 80 s, a steady-state is reached. An average value of 1.44 is reached over a longer period of time. It was interesting to observe that the measurement of friction coefficient is more stable and constant for dc than with pulse deposited samples, with less fluctuation observed.

High coefficient of friction observed for pulse plated Ni is due to its high hardness that results in wear of ball material itself. Average diameter of the worn out area of the ball was approximately 613 μm as shown in the optical image of Fig. 9a. Removal of ball

Table 1
Typical surface properties obtained for dc and pulse electrodeposited Ni.

	DC electrodeposited Ni current density: 50 mA/cm^2 deposition time: 20 min	Pulse electrodeposited Ni current density: 690 mA/cm^2 deposition time: 20 min
Average grain size at deposit surface	1 μm	100 nm
Texture	(2 0 0) preferred orientation	(2 0 0) preferred orientation with increased contribution from (1 1 1) planes
Residual stress, MPa Ni (3 1 1), iso-inclination method	−143 to −842 [15] (compressive)	−207 (compressive)
Vickers microhardness, VHN (microhardness tester)	226	310
Vickers hardness, VHN (nanoindenter)	230	313
Nanoindentation hardness, H_S (MPa)	2492 ± 214	3384 ± 297
Creep, C_S (%)	2.38	3.36
Modulus of elasticity, E_S (GPa)	262 ± 22	226 ± 21
Microscratch test, 30 N	No de-cohesion or cracking	No de-cohesion or cracking
Co-efficient of friction, μ	1.44	1.52
Wear rate (mm^3/N m)	8.18×10^{-5}	5.24×10^{-4}

Table 2
Values of coefficient of friction for Ni in literature.

Material	Coefficient of friction, μ	Wear rate ($mm^3/N\,m$)
Ni–P coatings (measured with Si_3N_4) [26]	0.7	5.5×10^{-3}
Ni	0.87	3.92×10^{-5}
Ni–8.39W (at%)	0.80	2.27×10^{-5}
Ni–9.43W	0.73	1.88×10^{-5}
Ni–12.70W (measured with 100Cr6 steel) [27]	0.82	1.14×10^{-5}
Ni–steel [28]	0.8 (fretting)	–
Ni–steel [29]	0.18–0.65 (fretting)	–
Ni–steel [30]	0.70	–
Ni composites–steel [31]	0.70–1.3	–

material causes significant fluctuation in coefficient values and high average values are obtained due to the formation of third body material composed of a mixture of worn out ball and Ni deposit, as shown in the SEM/EDS spectrum of Fig. 9b. Friction coefficient values of Ni found in literature [26–31] are given in Table 2 for comparison.

Wear track of pulse Ni was not uniform as shown in the profilometer curve of Fig. 10a compared to that of dc plated Ni shown in Fig. 10b. Average worn out area in pulse Ni sample was 5241 μm^2 compared to 818 μm^2 in dc plated Ni. Wear rates calculated from these curves for pulse and dc Ni were 5.24×10^{-4} and 8.18×10^{-5} $mm^3/N\,m$, respectively. Fine grains in pulse Ni sample could serve to trap wear debris thus increasing the real contact area between the pin and disc and thereby resulting in an increased wear rate due to third body abrasion [32]. Probability of grain pull-out from the surface of dc plated Ni is less due to their coarse size, resulting in less wear rate.

4. Conclusions

Pulse electrodeposition produced finer Ni grains compared to dc plating. Size of Ni grains increased with an increase in the duration of electrodeposition. Both DC and pulse deposition resulted in Ni with preferred (2 0 0) orientation but presence of (1 1 1) oriented grains increased in pulse plated Ni. Compressive residual stress was measured in pulse deposited Ni. Pulse plated Ni exhibited higher nanoindentation hardness, creep and coefficient of friction and lower modulus of elasticity than dc plated Ni.

Acknowledgements

The authors wish to acknowledge the support of Center of Research Excellence in Corrosion (CoRE-C) and the Ministry of Higher Education, Saudi Arabia. Assistance provided by Research Institute at the King Fahd University of Petroleum & Minerals, Dhahran, Saudi Arabia is also appreciated. We are also thankful to Dr. Philippe Kemp for his assistance in tribometer tests.

References

[1] D. Pletcher, F.C. Walsh, Industrial Electrochemistry, 2nd ed., Chapman and Hall, London, 1990.
[2] J.K. Dennis, T.E. Such, Nickel and Chromium Plating, Butterworth, London, 1986.
[3] H. Zhao, L. Liu, J. Zhu, Y. Tang, W. Hu, Mater. Lett. 61 (2007) 1605–1608.
[4] J.R. Tuck, A.M. Korsunsky, R.I. Davidson, S.J. Bull, D.M. Elliott, Surf. Coat. Technol. 127 (2000) 1.
[5] K.C. Chan, W.K. Chan, N.S. Qu, J. Mater. Process. Technol. 89–90 (1999) 447.
[6] A.M. El-Sherik, U. Erb, J. Mater. Sci. 30 (1995) 5743.
[7] A. Alfantazi, U. Erb, Scr. Metall. Mater. 30 (1994) 1245.
[8] C. Cheung, U. Erb, G. Palumbo, Mater. Sci. Eng. A185 (1994) 39.
[9] U. Erb, Nanostruct. Mater. 6 (1995) 533.
[10] D.H. Jeong, F. Gonzalez, G. Palumbo, K.T. Aust, U. Erb, Scr. Mater. 44 (2001) 493.
[11] P. Gyftou, E.A. Pavlatou, N. Spyrellis, Appl. Surf. Sci. 254 (18) (2008) 5910.
[12] X.-S. Liang, J.-H. Ouyang, Y.-F. Li, Y.-M. Wang, Appl. Surf. Sci. 255 (7) (2009) 4316.
[13] S.A. Lajevardi, T. Shahrabi, Appl. Surf. Sci. 256 (22) (2010) 6775.
[14] X. Yuan, D. Sun, H. Yu, H. Meng, Appl. Surf. Sci. 255 (6) (2009) 3613.
[15] R.J.C. Choo, J.M. Toguri, A.M. El-Sherik, U. Erb, J. Appl. Electrochem. 25 (1995) 384.
[16] C. Yang, Z. Yang, M. An, J. Zhang, Z. Tu, C. Li, Plat. Surf. Finish. 88 (5) (2001) 116.
[17] A. Ul-Hamid, A. Quddus, F.K. Al-Yousef, A.I. Mohammed, H. Saricimen, L.M. Al-Hadhrami, Surf. Coat. Technol. 205 (2010) 2023–2030.
[18] A. Cziraki, I. Gerocs, B. Fogarassy, E. Toth-Kadar, I. Bakonyi, J. Mater. Sci. 29 (1994) 4771.
[19] J.X. Kang, W.Z. Zhao, G.F. Zhang, Surf. Coat. Technol. 203 (13) (2009) 1815–1818.
[20] A.M. El-Sherik, J. Shirokoff, U. Erb, J. Alloys Compd. 389 (2005) 140.
[21] U. Klement, L. Hollang, S.R. Dey, M. Battabyal, O.V. Mishin, W. Skrotzki, Texture Anisotropy Polycryst. III Solid State Phenom. Ser. 160 (2010) 235–240.
[22] V.F.C. Lins, E.S. Cecconello, T. Matencio, J. Mater. Eng. Perform. 17 (5) (2008) 741–745.
[23] A.M. El-Sherik, U. Erb, J. Page, Surf. Coat. Technol. 88 (1996) 70–78.
[24] C.O. Rudd, R.J. McDowell, D.J. Snoha, Powder Diffract. 1 (1986) 22.
[25] W.C. Oliver, G.M. Pharr, J. Mater. Res. 7 (3) (1992) 1564.
[26] Q.-J. Zhou, J.-Q. Zhao, F. Nie, W.-Y. Chua, J.-X. Li, L.-J. Qiao, Wear 266 (2009) 810–813.
[27] A.S.M.A. Haseeb, U. Albers, K. Bade, Wear 264 (2008) 106–112.
[28] A.S.M.A. Haseeb, J.P. Celis, J.R. Roos, Thin Solid Films 444 (2003) 199–207.
[29] R. Mishra, B. Basu, R. Balasubramaniam, Mater. Sci. Eng. A 373 (2004) 370–373.
[30] S.M. Myers, J.A. Knapp, D.M. Follstaedt, M.T. Dugger, T.R. Christenson, Surf. Coat. Technol. 103–104 (1998) 287–292.
[31] X.H. Chen, C.S. Chen, H.N. Xiao, H.B. Liu, L.P. Zhou, S.L. Li, G. Zhang, Tribol. Int. 39 (2006) 22–28.
[32] F. Xiong, R. Manory, L. Ward, M. Terheci, J. Am. Ceram. Soc. 80 (1997) 1310–1312.